Creep and Shrinkage Effects in Spliced Prestressed Concrete Girder Bridges

Gregor P. Wollmann, Ph.D., P.E.
Senior Project Engineer
Michael Baker Jr., Inc.
Charleston, West Virginia

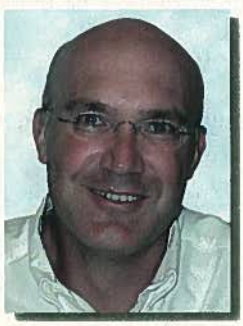

Robert B. Anderson, P.E.
Senior Structural Engineer
URS Corporation
Tampa, Florida

Carin L. Roberts-Wollmann, Ph.D., P.E.
Assistant Professor
Virginia Polytechnic Institute and State University
Blacksburg, Virginia

This paper reviews and demonstrates the age-adjusted concrete modulus approach to the time-dependent analysis of spliced precast concrete girder composite bridges. The method is illustrated by example of one of the post-tensioned spliced girder bridges built during the recently completed I-15 Reconstruction Project in Salt Lake City, Utah. Sixteen simple-span bridges up to 67 m (220 ft) in span length were constructed using a 2400 mm (94.5 in.) deep modified girder developed by the Washington State Department of Transportation. With a more accurate method for prestress loss calculations for such bridges, designers can take advantage of the higher concrete age at time of post-tensioning and the resultant reduction in creep and shrinkage strains.

The reconstruction of 27 km (17 miles) of Interstate I-15 in Salt Lake City, Utah, required rebuilding of 130 bridges in a timeframe of only $4^1/_2$ years for completion before the 2002 Winter Olympic Games. Using the innovative design-build project delivery system to its full advantage, the winning team was able to develop unique solutions for many of the challenges on the project.

One of these challenges was spanning a series of single-point urban interchanges, where the complex traffic pattern required simple-span bridges ranging in span length from 64 to 67 m (210 to 220 ft). For 16 of these interchanges, a scheme using spliced precast and post-tensioned concrete girders was adopted[1] (see Fig. 1). These girders were based on a 2400 mm (94.5 in.) deep bulb-tee section recently de-

Fig. 1. Bridge over single-point urban interchange (I-15, Salt Lake City, Utah).

veloped by the Washington State Department of Transportation.[2,3]

Due to the great depth of the girders, and in order to optimize their design, particular attention was paid to the long-term effects of creep and shrinkage. While the analysis results indicated that the effect of differential creep and shrinkage between deck and girders was negligible, significant economies could be achieved by taking advantage of the higher concrete age at time of girder post-tensioning and the resultant reduction in long-term prestress losses.

This paper reviews the theoretical background of the approximate analysis method used and presents its application to one of the I-15 spliced prestressed concrete girder bridges. The method takes advantage of the concept of the age-adjusted concrete modulus that was first introduced by Trost and further developed by Bazant.[4,5] With this approach, the complex creep and shrinkage laws can be linearized, which leads to a relatively simple set of equations that describe the long-term behavior of the composite system. While the method presented is not suitable for hand calculations, it can be easily implemented in a computer spreadsheet program.

The theoretical foundations for the time-dependent analysis of steel or precast concrete girders composite with a concrete deck have been developed over the past 50 years.[4-8] Reference 9 includes a summary which forms the basis of the presentation in this paper.

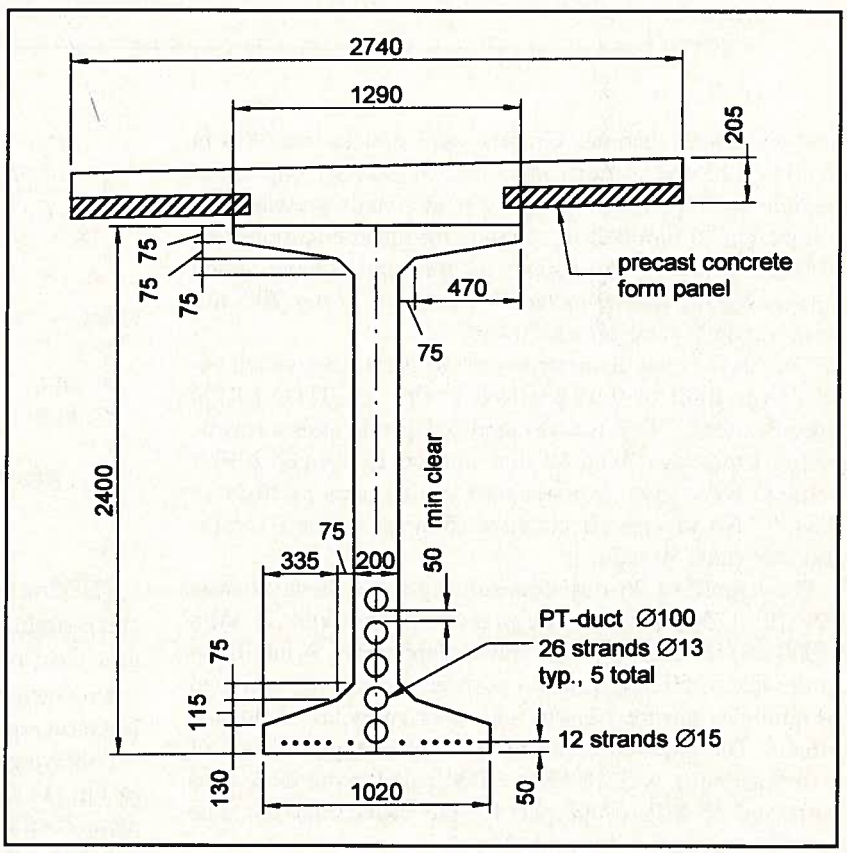

Fig. 2. Partial section of the I-15 Southbound Bridge over 7200 South.

Project Description

Fig. 2 shows a partial cross section of one of the spliced girder bridges of the project – the I-15 Southbound Bridge over 7200 South. The girder is 2400 mm (94.5 in.) deep and has a 200 mm ($7^7/_8$ in.) thick web which accommodates five

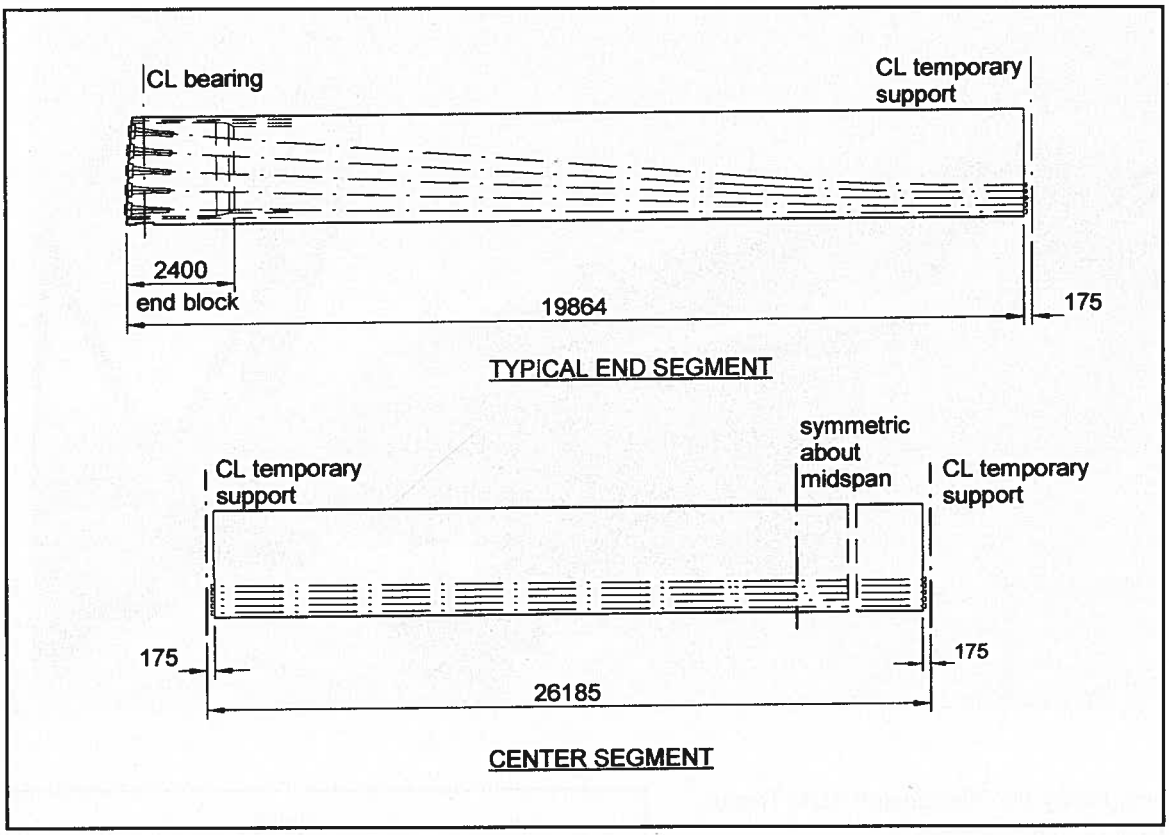

Fig. 3. Elevation of end segments and center segment.

post-tensioning tendons. Girders were cast in two 20.0 m (65.6 ft) long end sections and a 26.2 m (86.0 ft) long center section (see Fig. 3). The girder was nominally pretensioned using eight 15 mm (0.6 in.) strands for the end sections and twelve 15 mm (0.6 in.) strands for the center section. Each post-tensioning tendon included twenty-six 13 mm (0.5 in.) strands, Grade 1860 MPa (270 ksi).

The ratio of duct diameter to web width is 0.50, which exceeds the limit of 0.4 specified in the AASHTO LRFD Specifications.[10] This was deemed acceptable after a review of the literature revealed that numerous spliced girder bridges have been constructed with ratios as high as 0.54.[11,12] No adverse effects were observed on the I-15 project with the 0.50 ratio.

The specified 28-day concrete cylinder strength was 52 MPa (7500 psi) for the precast girders and 35 MPa (5000 psi) for deck slab and splice diaphragms. A minimum girder age of 50 days prior to post-tensioning was specified to minimize prestress losses and other creep and shrinkage effects. The required concrete cylinder strength at time of post-tensioning was 28 MPa (4000 psi) for the deck concrete and 35 MPa (5000 psi) for the splice concrete. The erection sequence is shown in Fig. 4.

CREEP AND SHRINKAGE EFFECTS IN COMPOSITE GIRDERS

The time-dependent strain in a concrete fiber can be expressed as the sum of elastic and creep strains due to the initial stress, elastic and creep strains due to changes in stress, and the shrinkage strain:

$$\varepsilon_t = \frac{\sigma_0}{E_0}\left(1+\varphi_{t,t_0}\right) + \int_{t_0}^{t}\left\{\frac{1}{E(\tau)}\frac{d\sigma(\tau)}{d\tau}\left[1+\varphi(t,\tau)\right]\right\}d\tau + \varepsilon_{s,t} \quad (1)$$

where

ε_t = total strain at time t
σ_0, $\sigma(\tau)$ = stress at time t_0 and τ, respectively
E_0, $E(\tau)$ = modulus of elasticity at times t_0 and τ, respectively
φ_{t,t_0}, $\varphi(t, \tau)$ = creep coefficient at time t due to load applied at time t_0 and τ, respectively
$\varepsilon_{s,t}$ = shrinkage strain at time t

The first term of the equation represents the elastic and creep strains due to a stress σ_0 applied at time t_0. The integral term represents the elastic and creep strains due to stress changes $(d\sigma/dt)d\tau$ in the time interval from t_0 to t. The last term represents the shrinkage strain at time t.

Following the method proposed by Trost, the integral term in Eq. (1) can be replaced by an algebraic expression if an aging coefficient μ is introduced.[4,5] This greatly simplifies the equation, yielding Eq. (2):

$$\varepsilon_t = \frac{\sigma_0}{E_0}\left(1+\varphi_{t,t_0}\right) + \frac{\sigma_t-\sigma_0}{E_0}\left(1+\mu\varphi_{t,t_0}\right) + \varepsilon_{s,t} \quad (2)$$

where σ_t is the stress at time t.

Comparing Eqs. (1) and (2), it follows that the aging coefficient μ is given by Eq. (3):

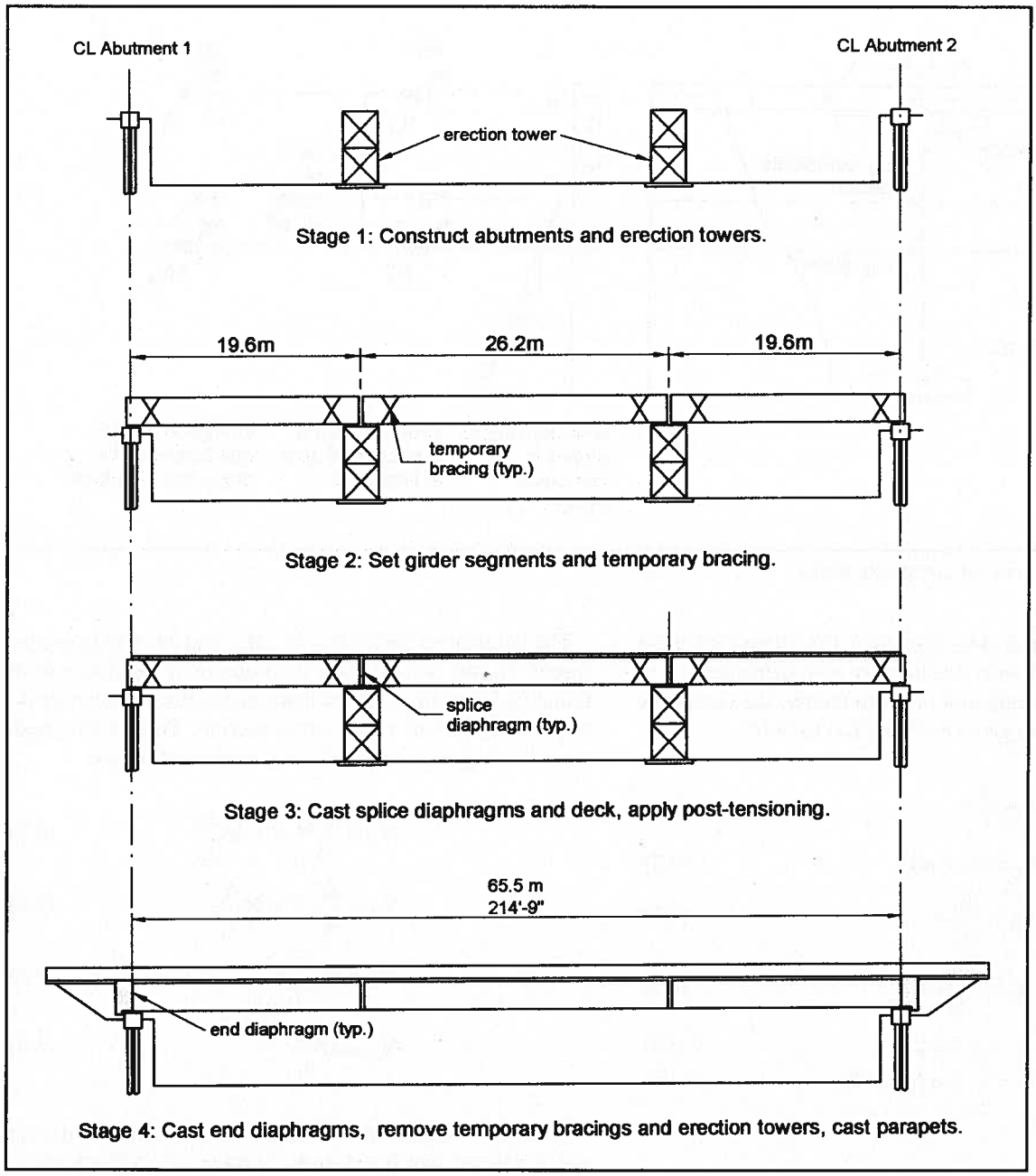

Fig. 4. Erection sequence.

$$\mu = \frac{E_0}{(\sigma_t - \sigma_0)\varphi_{t,t_0}} \int_{t_0}^{t} \frac{1}{E(\tau)} \frac{d\sigma(\tau)}{d\tau} [1 + \varphi(t,\tau)]\, d\tau - \frac{1}{\varphi_{t,t_0}} \tag{3}$$

Thus, the aging coefficient is a complex function of the load history $\sigma(\tau)$ and of the time-dependent concrete properties. The coefficient accounts for the reduced creep of concrete loaded at a greater age. The upper bound for μ is 1.0, corresponding to the case where the load history is a single step stress increment $\Delta\sigma = \sigma_t - \sigma_0$ applied at time $t = t_0$ with no further changes.

Bazant[4] has shown that when the change in stress is induced by creep and shrinkage, μ ranges from approximately 0.5 to almost 1.0. For first loading occurring at a concrete age between 10 and 100 days, a value between 0.7 and 0.9 is appropriate.

By using a single, constant aging coefficient, creep and shrinkage calculations are significantly simplified and can be reduced to the solution of a set of linear equations. Given that creep and shrinkage properties are subject to large scatter and cannot be determined with great accuracy, such a simplification is justified. Note that in Eq. (2), the aging coefficient is multiplied by the creep coefficient. Therefore, given the variability of the creep properties, an especially high accuracy for the aging coefficient is not required.

Composite Girder System

Fig. 5 shows the conditions in a composite girder system. It is useful to decompose the internal forces acting on the composite section, M^0 and N^0, into forces and moments acting separately on the girder and deck. Thus, M_D^0, N_D^0, M_G^0 and N_G^0 are the initial creep-producing stress resultants and

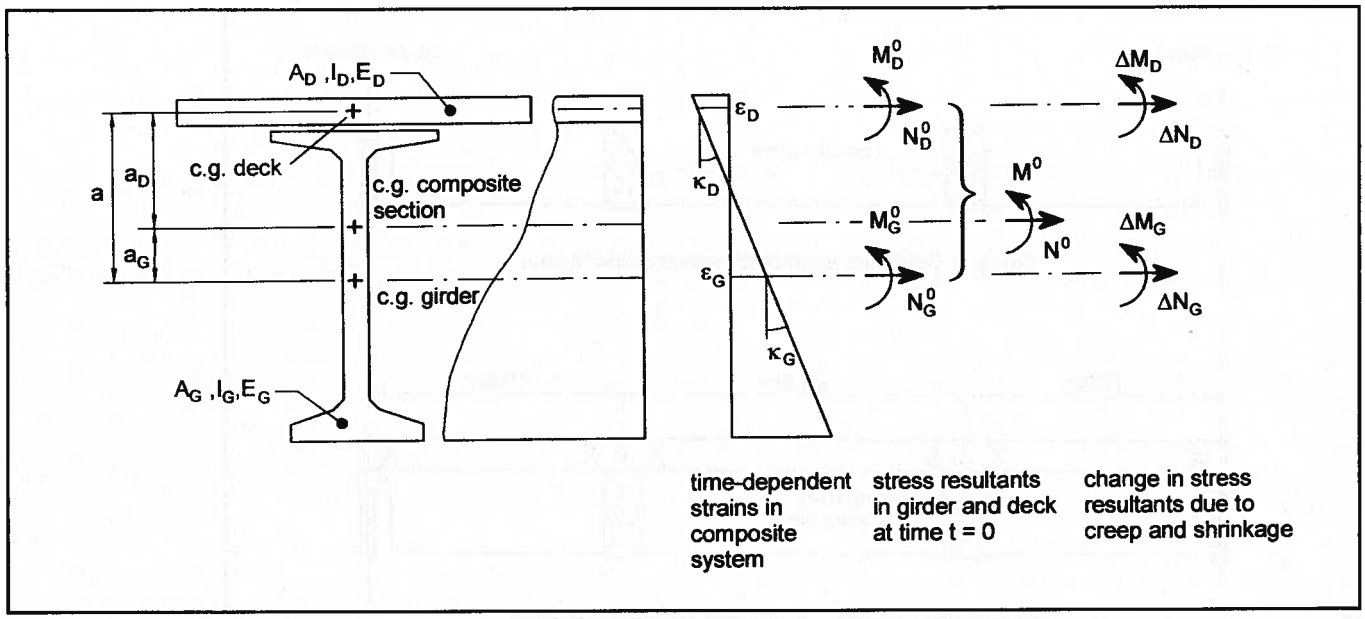

Fig. 5. Strains and forces for composite girder.

ΔM_D, ΔN_D, ΔM_G and ΔN_G represent the change to these stress resultants with time due to creep and shrinkage.

With the usual assumption of beam theory, the composite section properties are given by Eqs. (4.1) to (4.6):

$$n = \frac{E_D}{E_G} \tag{4.1}$$

$$A_C = A_G + nA_D \tag{4.2}$$

$$a_D = \frac{A_G}{A_C} a \tag{4.3}$$

$$a_G = \frac{nA_D}{A_C} a \tag{4.4}$$

$$S_C = n A_D a_D \tag{4.5}$$

$$I_C = I_G + n I_D + a S_c \tag{4.6}$$

where

n = modular ratio of deck concrete to girder concrete

E_D, E_G = modulus of elasticity for deck and girder, respectively

A_D, A_G = area of deck and girder, respectively

A_C = area of transformed composite section

a = distance between centroid of deck and centroid of girder

a_D = distance between centroid of deck and centroid of composite section

a_G = distance between centroid of girder and centroid of composite section

S_C = first area moment of the transformed deck section about the centroid of the composite section

I_D, I_G = moment of inertia of deck and girder, respectively, about their own centroids

I_C = moment of inertia of the composite section about its centroid

The component forces N_D, N_G, M_D, and M_G due to section forces M and N acting on the composite section can be found by integrating the resultant stress distribution over the respective portions of the cross section. This action yields the following expressions for the component forces:

$$N_D = \frac{n A_D}{A_C} N - M \frac{S_C}{I_C} \tag{5.1}$$

$$N_G = \frac{A_G}{A_C} N + M \frac{S_C}{I_C} \tag{5.2}$$

$$M_D = M \frac{n I_D}{I_C} \tag{5.3}$$

$$M_G = M \frac{I_G}{I_C} \tag{5.4}$$

With time, strains and curvature will change due to creep and shrinkage, which causes the build-up of a self-equilibrating state of stress over the cross section. This time-dependent change is described by eight unknown quantities – ΔM_D, ΔN_D, ΔM_G, ΔN_G, κ_D, ε_D, κ_G, and ε_G – as shown in Fig. 5.

To obtain a unique solution, eight equations are needed. Two of these equations – Eqs. (6.1) and (6.2) – can be found from compatibility requirements, assuming plane sections remain plane and perfect bond between deck and girder:

$$\kappa_G = \kappa_D = \kappa \tag{6.1}$$

$$\varepsilon_D = \varepsilon_G - \kappa a \tag{6.2}$$

Two additional equations are given by equilibrium requirements:

$$\Delta N_D + \Delta N_G = 0 \tag{6.3}$$

$$\Delta M_D + \Delta M_G + \Delta N_G a = 0 \tag{6.4}$$

Eqs. (6.3) and (6.4) signify that, even though stresses will change in time, there is no resultant force on the composite section due to these changes – i.e., the time-dependent stresses are self-equilibrating. This is true for a statically determinate system where long-term deformations do not cause a change in section forces. For an indeterminate structure, Eqs. (6.3) and (6.4) would need to be modified to include terms for the time-dependent redundant forces.

The remaining four equations are given by the constitutive equations describing the time-dependent strains, analogous to Eq. (2):

$$\varepsilon_D = \frac{N_D^0}{E_D A_D}\varphi_D + \frac{\Delta N_D}{E_D A_D}(1+\mu\varphi_D) + \varepsilon_{sD} \qquad (6.5)$$

$$\varepsilon_G = \frac{N_G^0}{E_G A_G}\varphi_G + \frac{\Delta N_G}{E_G A_G}(1+\mu\varphi_G) + \varepsilon_{sG} \qquad (6.6)$$

$$\kappa_D = \frac{M_D^0}{E_D I_D}\varphi_D + \frac{\Delta M_D}{E_D I_D}(1+\mu\varphi_D) \qquad (6.7)$$

$$\kappa_G = \frac{M_G^0}{E_G I_G}\varphi_G + \frac{\Delta M_G}{E_G I_G}(1+\mu\varphi_G) \qquad (6.8)$$

where

φ_D, φ_G = creep coefficient for deck and girder, respectively

ε_{sD}, ε_{sG} = shrinkage strain for deck and girder, respectively

Note that Eqs. (6.5) to (6.8) do not include initial strains – i.e., they describe time-dependent strains only.

Input data required for the solution of this system of equations are cross section and material properties (E_D, E_G, A_D, A_G, I_D, I_G, and a), creep-producing stress resultants (N_D^0, N_G^0, M_D^0 and M_G^0), and creep and shrinkage values (φ_D, ε_{sD}, φ_G, ε_{sG}, and μ). While cumbersome to do by hand, solving this system of equations is well within the capabilities of commercially available computer spreadsheet or mathematical analysis programs.

Effect of Prestress Losses

The effect of prestress and prestress losses can be implemented easily in the system of equations. The initial prestress force is considered with the creep-producing stress resultants M_D^0, M_G^0, N_D^0 and N_G^0. Prestress losses are initially estimated by guessing at the time-dependent change in strain, ε_p, at the location of the tendons or strands. The forces acting on the composite section due to prestress losses are then given by Eqs. (7.1) and (7.2):

$$\Delta N^P = A_{ps}(\Delta f_R - E_{ps}\varepsilon_p) \qquad (7.1)$$

$$\Delta M^P = \Delta N^P e \qquad (7.2)$$

where

A_{ps} = cross-sectional area of prestressing steel

E_{ps} = modulus of elasticity of prestressing steel

ε_p = time-dependent change in strain at location of prestressing steel (tension positive)

Δf_R = prestress loss due to strand relaxation

e = eccentricity of prestressing steel relative to centroid of composite section (down positive)

Forces ΔN^P and ΔM^P can be decomposed into component forces ΔN_D^P, ΔM_D^P, ΔN_G^P and ΔM_G^P in the deck and girder by applying Eqs. (5.1) to (5.4). The component forces due to prestress losses are self-equilibrating with the change in tendon force. Therefore, Eqs. (6.3) and (6.4) remain unchanged. Furthermore, the assumption of plane sections remaining plane still applies [Eqs. (6.1) and (6.2)]. Only Eqs. (6.5) to (6.8) need to be modified to account for prestress losses:

$$\varepsilon_D = \frac{N_D^0}{E_D A_D}\varphi_D + \frac{\Delta N_D + \Delta N_D^P}{E_D A_D}(1+\mu\varphi_D) + \varepsilon_{sD} \qquad (8.1)$$

$$\varepsilon_G = \frac{N_G^0}{E_G A_G}\varphi_G + \frac{\Delta N_G + \Delta N_G^P}{E_G A_G}(1+\mu\varphi_G) + \varepsilon_{sG} \qquad (8.2)$$

$$\kappa_D = \frac{M_D^0}{E_D I_D}\varphi_D + \frac{\Delta M_D + \Delta M_D^P}{E_D I_D}(1+\mu\varphi_D) \qquad (8.3)$$

$$\kappa_G = \frac{M_G^0}{E_G I_G}\varphi_G + \frac{\Delta M_G + \Delta M_G^P}{E_G I_G}(1+\mu\varphi_G) \qquad (8.4)$$

Combining Eqs. (6.1) to (6.4) and (8.1) to (8.4) and substituting $\kappa = \kappa_D = \kappa_G$ yields, after some rearranging, the system of seven equations and seven unknowns [Eqs. (9.1) to (9.7)] shown at the bottom of this page.

$$\begin{bmatrix} E_G A_G & -E_G A_G & aE_G A_G & 0 & 0 & 0 & 0 \\ 0 & 0 & 0 & 1 & 1 & 0 & 0 \\ 0 & 0 & 0 & 0 & a & 1 & 1 \\ E_D A_D & 0 & 0 & -(1+\mu\varphi_D) & 0 & 0 & 0 \\ 0 & E_G A_G & 0 & 0 & -(1+\mu\varphi_G) & 0 & 0 \\ 0 & 0 & E_D I_D & 0 & 0 & -(1+\mu\varphi_D) & 0 \\ 0 & 0 & E_G I_G & 0 & 0 & 0 & -(1+\mu\varphi_G) \end{bmatrix} \begin{bmatrix} \varepsilon_D \\ \varepsilon_G \\ \kappa \\ \Delta N_D \\ \Delta N_G \\ \Delta M_D \\ \Delta M_G \end{bmatrix} = \begin{bmatrix} 0 \\ 0 \\ 0 \\ N_D^0\varphi_D + \Delta N_D^P(1+\mu\varphi_D) + E_D A_D \varepsilon_{sD} \\ N_G^0\varphi_G + \Delta N_G^P(1+\mu\varphi_G) + E_G A_G \varepsilon_{sG} \\ M_D^0\varphi_D + \Delta M_D^P(1+\mu\varphi_D) \\ M_G^0\varphi_G + \Delta M_G^P(1+\mu\varphi_G) \end{bmatrix}$$

(9.1) to (9.7)

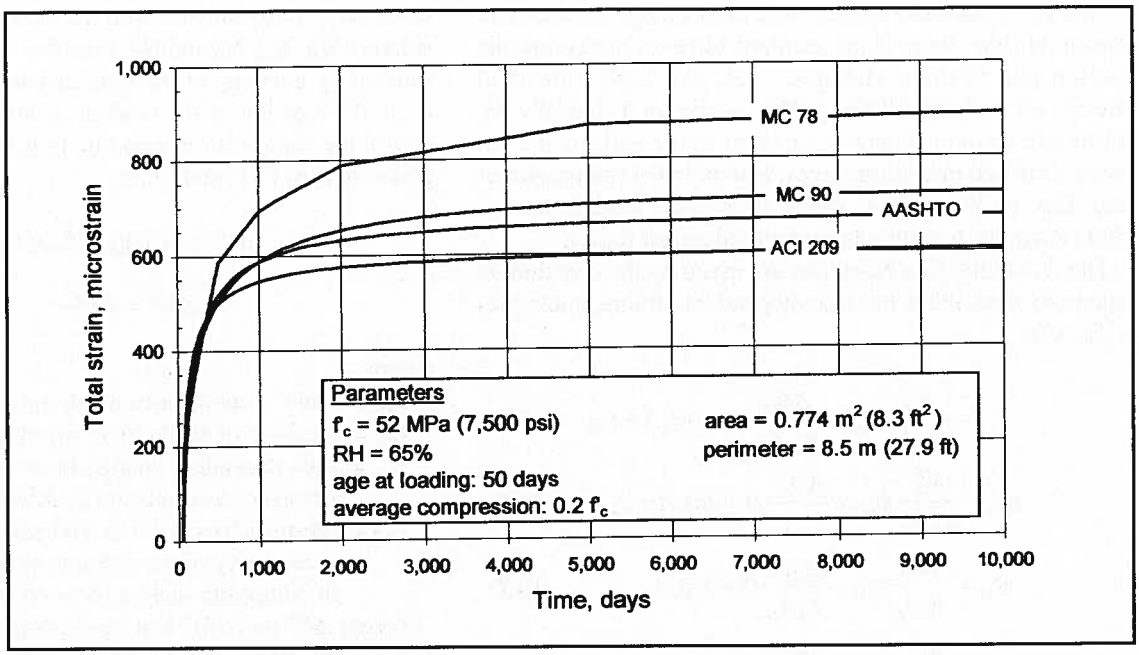

Fig. 6. Comparison of creep and shrinkage models.

After the system of equations has been solved, the time-dependent strains are known and the initial assumption for the prestress losses can be verified. If necessary, the assumption is corrected and new strains are calculated. This iterative scheme converges rapidly, because the influence of the prestress losses on the time-dependent strains is typically quite small. Some spreadsheet programs have a built-in solve routine that can be used to perform the iteration.

Section Properties

The effects of girder reinforcement and pretensioning strands can be readily considered in the analysis. This only requires that quantities A_G, I_G, and a_G in Eqs. (4.1) to (4.6) be determined using the transformed section properties of the girder-strand-rebar system.

With precast post-tensioned girders, the tendon ducts represent a fairly large portion of the overall section and, therefore, have some influence on the section properties. In many cases, the use of gross section properties will be acceptable. However, for a more accurate determination of extreme fiber stresses, net section properties accounting for the duct areas should be used for load cases active prior to grouting of the tendons. Loads applied after curing of the grout act on the transformed section including the post-tensioning strands. Eqs. (4.1) to (4.6) are still applicable with the appropriate values input for the net or transformed (grouted) girder section properties.

Eqs. (8.1) to (8.4) need to be modified. Eq. (10), for example, is the resultant equation of modifying Eq. (8.2). Modification of Eqs. (8.1), (8.3), and (8.4) is analogous.

$$\varepsilon_G = \left[\frac{N_G^0}{E_G A_G}\varphi_G\right]_{net} + \left[\frac{N_G^0}{E_G A_G}\varphi_G\right]_{grouted} + \left[\frac{\Delta N_G + \Delta N_G^P}{E_G A_G}(1+\mu\varphi_G)\right]_{grouted} + \varepsilon_{sG} \quad (10)$$

The first term ("net") includes the portion of the girder force N_G^0 acting prior to grouting of the ducts. The creep coefficient φ_G in that term depends on the concrete age at time of application of this load. The quantity A_G is based on the net section of the girder, deducting the holes for the post-tensioning ducts. The effect of reinforcing steel and pretensioning steel may be included by transforming their areas based on the ratio of girder concrete modulus and steel modulus.

Similarly, the second and third terms ("grouted") refer to load effects, section properties, and creep coefficient after curing of the grout in the post-tensioning ducts. It is assumed that grouting takes place shortly after post-tensioning so that all redistribution forces, ΔN_G and ΔN_G^P, act on the transformed section, including the post-tensioning strands.

There will be a small redistribution of compressive stresses from the girder concrete to the grout in the tendon ducts [this has been ignored in the formulation of Eq. (10)]. This redistribution is caused by the difference in long-term strains between the non-prestressed grout and the surrounding prestressed girder concrete.

In general, the use of gross section properties instead of net and transformed section properties as appropriate will be conservative for two reasons:

1. The post-tensioning force acts on the net section; therefore, the beneficial effect of post-tensioning is underestimated when gross section properties are used.

2. Additional loads applied after grouting of the tendons act on the transformed section. Using gross section properties and thereby ignoring the contribution of the strands to the section properties will overestimate additional stresses.

Creep and Shrinkage Coefficients

A number of models are available to calculate creep coefficient and shrinkage strain. Among those in the United States are the AASHTO LRFD Specifications,[10] ACI

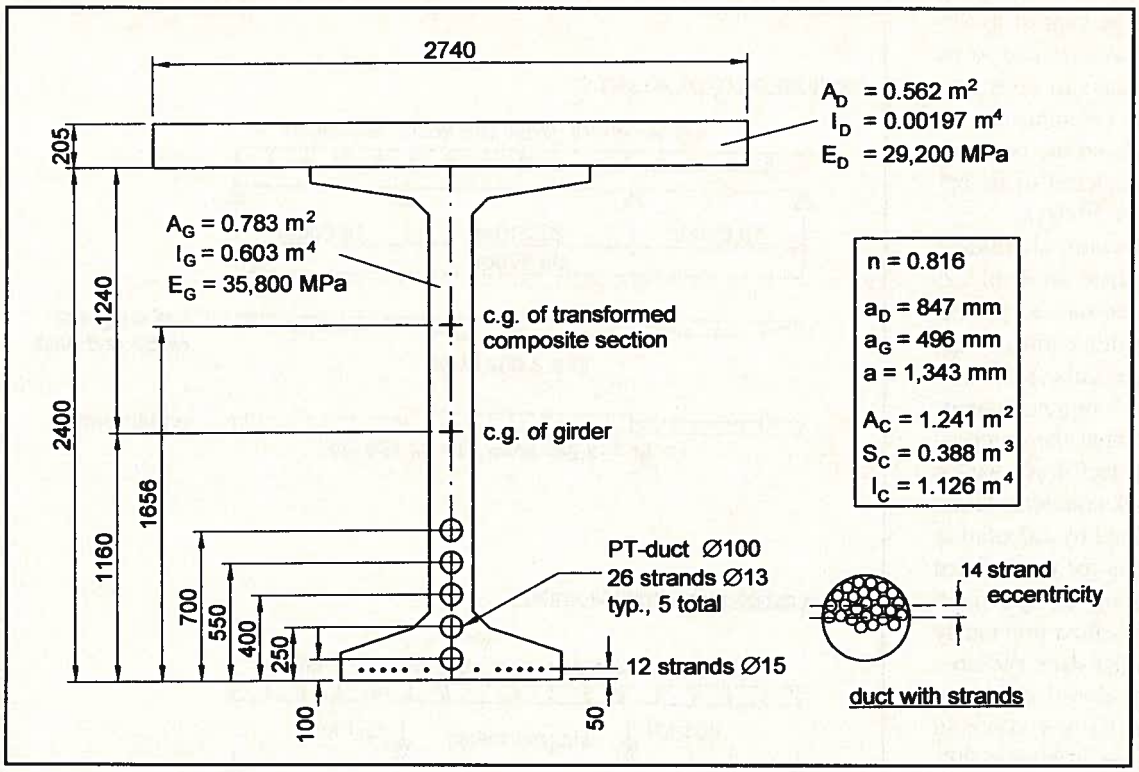

Fig. 7. Idealized cross section properties for interior girder (I-15 Southbound over 7200 South).

209R,[13] the 1990 CEB-FIP Model Code,[14] and the 1978 CEB-FIP Model Code.[15] The two CEB-FIP models have been used frequently for the design of segmental concrete bridges, probably as a consequence of the fact that many of the early analysis programs for this application originated in Europe.

Fig. 6 shows a comparison of creep and shrinkage strains based on these models with typical parameters for spliced girder bridges. With the exception of the 1978 CEB-FIP Model Code (MC 78 in the figure), total calculated strains show reasonably good agreement, varying by some 15 percent from low to high. However, although total strains may be comparable, there are significant differences when creep coefficients and shrinkage strains are compared separately. Furthermore, their development with time is different in the various models. The latter fact becomes particularly important with composite structures where the early time-dependent strains occur prior to the system being made composite.

In general, creep and shrinkage strains cannot be determined with good accuracy. Creep and shrinkage properties vary regionally, depending on the quality of the local concrete constituents. Therefore, the predicted values based on any of the methods listed above must be considered a best estimate subject to considerable variation. For critical cases, it is advisable to analyze the sensitivity of the results to changes in the input data. Improved predictions can be expected if creep and shrinkage properties are determined experimentally for a specific concrete mix. However, creep and shrinkage effects will rarely be critical for the spliced girder applications discussed here and, therefore, the use of the best estimate predictions should be adequate in many cases.

Table 1. Assumed erection schedule.

Day	Event	Age (days)		
		Girder	Deck panel	C.I.P. deck
1	Release pretensioning force	1	1	—
29	Erect girder	29	—	—
43	Cast deck	43	—	0
50	Post-tension and remove support	50	50	7
78	Apply superimposed dead load	78	78	35
10,000	Final	10,000	10,000	9957

Table 2. Creep coefficients and shrinkage strains (relative humidity = 65 percent).

Girder	Mean	90 percent fractile	Deck	Mean	90 percent fractile
$\varphi(10{,}000; 50)$	1.55	1.95	$\varphi(10{,}000; 7)$	1.97	2.48
$\varepsilon_s(10{,}000; 43)$	268×10^{-6}	391×10^{-6}	$\varepsilon_s(10{,}000; 1)$	351×10^{-6}	512×10^{-6}

Note: $\varphi_{90} = 1.26\varphi$; $\varepsilon_{s,90} = 1.46\varepsilon_s$.

DESIGN EXAMPLE

The following design example is for an interior girder of a representative bridge from the I-15 reconstruction project (I-15 Southbound over 7200 South). The idealized cross section and corresponding section properties are shown in Fig. 7. The slab haunch was neglected in the calculations and gross section properties were used.

Table 1 lists the assumed erection schedule. Post-tensioning and support removal was allowed to take place when the

deck had reached 80 percent of its 28-day strength. This was assumed to be the case after seven days of deck curing. To simplify the calculations, all creep-producing loads on the composite system were considered to be applied at a girder age of 50 days.

Creep coefficients and shrinkage strains are summarized in Table 2. These values were determined per the 1990 CEB-FIP Model Code.[14] The creep and shrinkage values for the deck listed in Table 2 represent averages to take into account the composite action of precast deck form panels and cast-in-place deck concrete. These values were determined by calculating long-term axial strains for the isolated composite deck using an approach analogous to that presented previously for the composite girder-deck system.

The analysis presented below is based on the mean values given in Table 2. The influence of the variability of creep and shrinkage properties is examined further on in the paper under "Sensitivity Analysis," where combinations of 90 percent fractile and mean values are used.

Fig. 8 shows loads and moment diagrams needed for the calculation of long-term effects. All post-tensioning tendons were stressed only from one end. However, due to the effect of wedge seating at the anchorages [assumed as 6 mm ($^3/_8$ in.)], the resulting prestressing force distribution was nearly symmetrical with a maximum at midspan. The assumed friction coefficient of 0.25 and the wobble of 0.0007/m (0.0002/ft) were confirmed on site by in-place friction tests for two of the tendons.

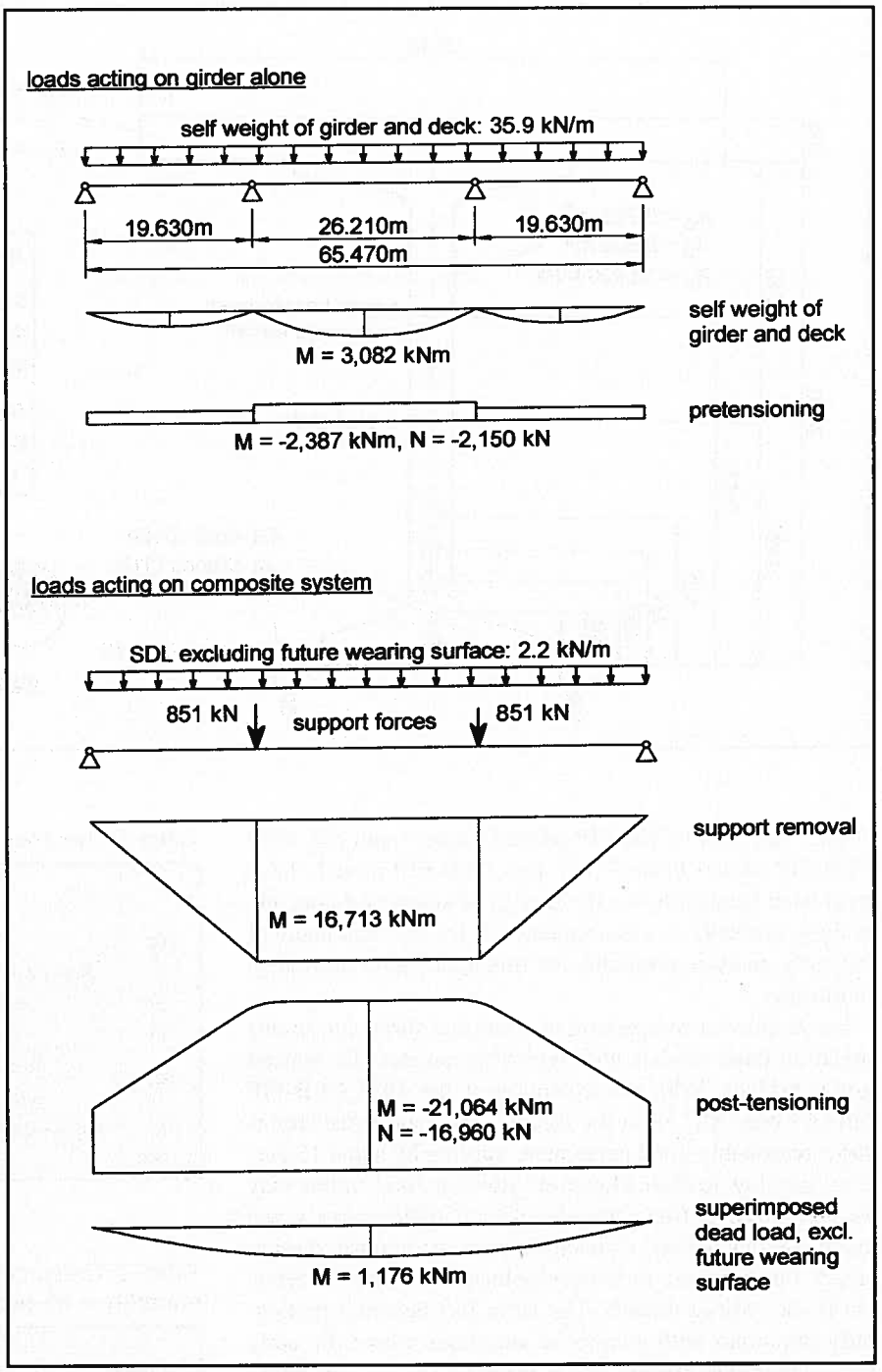

Fig. 8. Loads and moment diagrams needed for calculating long-term effects.

A summary of the creep-producing loads and the corresponding component section forces is provided by Tables 3 and 4. The prestressing forces are those acting at a girder age of 50 days – i.e., at the time when the system is made composite. Losses due to creep, shrinkage, and relaxation to Day 50 must be considered. For the prestressing strands, these losses were calculated as follows:

Stressing bed prestress (75 percent of nominal breaking strength) = 1395 MPa (202 ksi)

Relaxation prior to release = –11 MPa (–1.6 ksi)

Elastic shortening = –41 MPa (–5.9 ksi)

Losses between release and closure (50 days):

Creep [φ (50; 1) = 1.55, Reference 14] = –37 MPa (–5.4 kips)

Shrinkage [ε_s (50;1) = –72 x 10^{-6}, Reference 14] = –14 MPa (–2.0 ksi)

Relaxation = –12 MPa (–1.7 ksi)

Prestress at closure = 1280 MPa (185.7 ksi)

The corresponding force at midspan, acting on the girder alone, is:

12 strands × 140 mm^2 × 1280 MPa × 10^{-3} = –2150 kN (–483 kips)

The eccentricity (see Fig. 7) is:

1160 – 50 = 1110 mm = 1.11 m (43.7 in.)

The moment due to prestress is:

$-2150 \text{ kN} \times 1.11 \text{ m} = -2387 \text{ kN-m}$ (–1761 kip-ft)

Post-tensioning is applied at Day 50. The stress in the post-tensioning tendons at midspan after friction, seating, and elastic shortening losses was found to be 1322 MPa (191.7 ksi). The corresponding force, acting on the composite section, is:

$5 \text{ tendons} \times 26 \text{ strands} \times 98.7 \text{ mm}^2 \times 1322 \text{ MPa} \times 10^{-3} = -16{,}960 \text{ kN}$ (–3813 kips)

With the eccentricities shown in Fig. 7, the corresponding moment is:

$-16{,}960 \text{ kN} \times (1656 - 400 - 14) \text{ mm} \times 10^{-3} = -21{,}064 \text{ kN-m}$ (–15,537 kip-ft)

Using the iterative procedure described above, the change in strain from Day 50 to Day 10,000 at the location of the centroid of the post-tensioning tendons was found to be $\varepsilon_p = -756 \times 10^{-6}$, corresponding to a change in stress of:

$\Delta f_p = -756 \times 10^{-6} \times 200{,}000 \text{ MPa} = -151.2 \text{ MPa}$ (–21.9 ksi)

For the prestressing strands, the long-term strain change at the level of the strands was found to be -716×10^{-6}, corresponding to a change in stress of –143.2 MPa (–20.8 ksi).

The losses due to strand relaxation after making the deck composite with the girder need to be added to these values. According to Collins and Mitchell,[16] for low-relaxation strand, these losses may be calculated using Eq. (11):

$$\Delta f_R = 0.8 f_{pi} \frac{\log t}{45} \left(\frac{f_{pi}}{0.9 f_{pu}} - 0.55 \right) \quad (11)$$

where

t = time interval in hours
f_{pi} = initial steel stress
f_{pu} = nominal breaking strength of tendon

Therefore, for the prestressing strands, the relaxation loss between Day 50 (1200 hrs) and Day 10,000 (240,000 hrs) is:

$$\Delta f_R = 0.8 \times 1395 \frac{\log 240{,}000 - \log 1200}{45} \left(\frac{1395}{0.9 \times 1860} - 0.55 \right)$$

$$= 16 \text{ MPa (2.3 ksi)}$$

For the post-tensioning tendons, the relaxation loss is:

$$\Delta f_R = 0.8 \times 1322 \frac{\log 240{,}000}{45} \left(\frac{1322}{0.9 \times 1860} - 0.55 \right)$$

$$= 30 \text{ MPa (4.4 ksi)}$$

The forces acting on the composite section due to these prestress losses are:

Table 3. Creep producing loads.

		M (kN-m)	N (kN)
On girder (1)	DL	3082	0
	Pretensioning	–2387	–2150
	Total	696	–2150
On composite (2)	Post-tensioning	–21,064	–16,960
	Support removal	16,713	0
	SDL	1176	0
	Total	–3175	–16,960
Prestress losses on composite (3)	Post-tensioning loss	2888	2325
	Pretensioning loss	430	267

Note: 1 kN = 0.225 kips; 1 kN-m = 0.737 kip-ft.

Table 4. Component forces due to creep producing loads.

	Girder		Deck	
	N_G^0 (kN)	M_G^0 (kN-m)	N_D^0 (kN)	M_D^0 (kN-m)
Due to (1)*	–2150	696	0	0
Due to (2)*	–11,792	–1701	–5168	–5
Total	–13,942	–1005	–5168	–5
Post-tensioning loss*	2463	1,547	–137	4
Pretensioning loss*	317	231	–49	1
Total	2780	1778	–187	5

* See Table 3.
Note: 1 kN = 0.225 kips; 1 kN-m = 0.737 kip-ft.

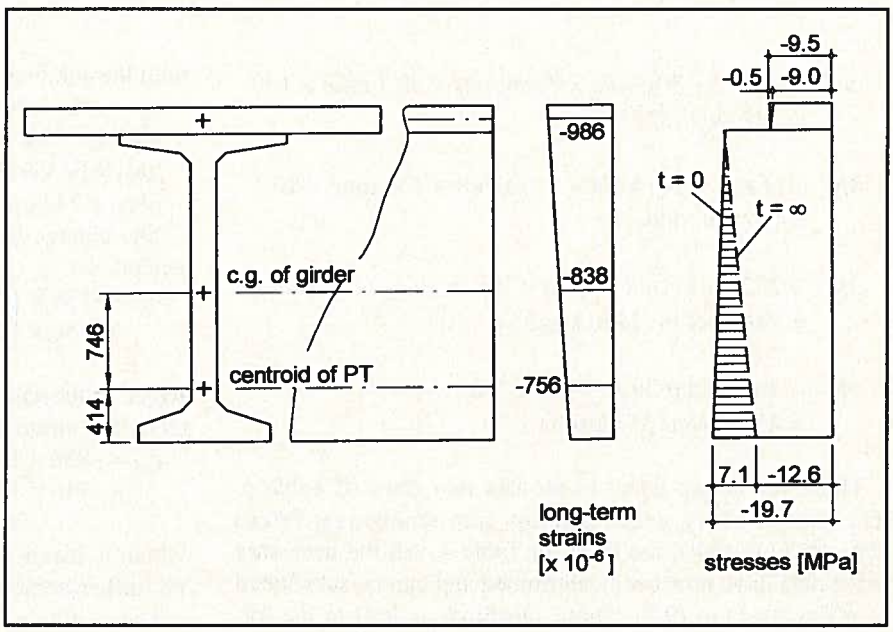

Fig. 9. Long-term strains and, initial and final stresses.

Table 5. Sensitivity of analysis results to variation of creep and shrinkage values.

	1a	1b	1c	2	3
φ_D	1.97	1.97	1.97	2.48	2.48
ε_{SD}	351×10^{-6}	351×10^{-6}	351×10^{-6}	512×10^{-6}	512×10^{-6}
φ_G	1.55	1.55	1.55	1.95	1.55
ε_{SG}	268×10^{-6}	268×10^{-6}	268×10^{-6}	391×10^{-6}	268×10^{-6}
μ	0.7	0.5	0.9	0.7	0.7

Deck	f_{top}	f_{bot}	f_{top}	f_{bot}	f_{top}	f_{bot}	f_{top}	f_{bot}	f_{top}	f_{bot}
$t = 0$	–9.0	–9.4	–9.0	–9.4	–9.0	–9.4	–9.0	–9.4	–9.0	–9.4
PT change*	–0.6	–0.1	–0.6	–0.1	–0.6	–0.1	–0.7	–0.1	–0.6	–0.1
CS change†	0.1	0.2	0.1	0.3	0.1	0.2	0.1	0.3	1.3	1.7
$t = \infty$	–9.5	–9.3	–9.5	–9.2	–9.5	–9.3	–9.5	–9.2	–8.2	–7.8
LL & FWS‡	–6.0	–4.8	–6.0	–4.8	–6.0	–4.8	–6.0	–4.8	–6.0	–4.8
Total	–15.5	–14.1	–15.5	–14.0	–15.5	–14.1	–15.5	–14.0	–14.2	–12.6

Girder	f_{top}	f_{bot}	f_{top}	f_{bot}	f_{top}	f_{bot}	f_{top}	f_{bot}	f_{top}	f_{bot}
$t = 0$	–15.7	–19.7	–15.7	–19.7	–15.7	–19.7	–15.7	–19.7	–15.7	–19.7
PT change*	–0.1	7.0	–0.1	7.3	–0.1	6.7	–0.1	8.5	–0.1	6.8
CS change†	–0.3	0.1	–0.4	0.1	–0.3	0.1	–0.5	0.2	–3.5	1.1
$t = \infty$	–16.2	–12.6	–16.2	–12.3	–16.1	–13.0	–16.4	–11.0	–19.3	–11.8
LL & FWS‡	–5.9	12.6	–5.9	12.6	–5.9	12.6	–5.9	12.6	–5.9	12.6
Total	–22.1	0	–22.1	0.3	–22	–0.4	–22.3	1.6	–25.2	0.8

* Stress change due to prestress losses.
† Stress change due to differential creep and shrinkage.
‡ Stresses due to live load and future wearing surface.
Note: 1 MPa = 145 psi.

$$\Delta N_1^P = (151.2 + 30)\text{ MPa} \times 90\text{ strands} \times 98.7\text{ mm}^2 \times 10^{-3} = 2325\text{ kN (523 kips)}$$

$$\Delta N_2^P = (143.2 + 16)\text{ MPa} \times 12\text{ strands} \times 140\text{ mm}^2 \times 10^{-3} = 267\text{ kN (60 kips)}$$

$$\Delta M_1^P = 2325\text{ kN}\,(1656 - 414) \times 10^{-3}\text{ m} = 2888\text{ kN-m (2130 kip-ft)}$$

$$\Delta M_2^P = 267\text{ kN}\,(1656 - 50) \times 10^{-3}\text{ m} = 430\text{ kN-m (317 kip-ft)}$$

These forces are listed in the last two rows of Table 3. The results of the decomposition into component forces [Eqs. (5.1) to (5.4)] are listed in Table 4. All the necessary input data have now been determined and can be substituted into Eqs. (9.1) to (9.7). These substitutions lead to the following system of equations:

$$\begin{bmatrix} 28.031 & -28.031 & 37.632 & 0 & 0 & 0 & 0 \\ 0 & 0 & 0 & 1 & 1 & 0 & 0 \\ 0 & 0 & 0 & 0 & 1.343 & 1 & 1 \\ 16.410 & 0 & 0 & -2.379 & 0 & 0 & 0 \\ 0 & 28.031 & 0 & 0 & -2.085 & 0 & 0 \\ 0 & 0 & 0.0575 & 0 & 0 & -2.379 & 0 \\ 0 & 0 & 21.587 & 0 & 0 & 0 & -2.085 \end{bmatrix} \begin{bmatrix} \varepsilon_D \\ \varepsilon_G \\ \kappa \\ \Delta N_D \\ \Delta N_G \\ \Delta M_D \\ \Delta M_G \end{bmatrix} = \begin{bmatrix} 0 \\ 0 \\ 0 \\ -16{,}384 \\ -23{,}327 \\ 2 \\ 2148 \end{bmatrix}$$

with the solution

$\varepsilon_D = -986 \times 10^{-6}$, $\varepsilon_G = -838 \times 10^{-6}$
$\kappa = 110 \times 10^{-6}$/m ($33.5 \times 10^{-6}$/ft)
$\Delta N_D = 84$ kN (19 kips), $\Delta N_G = -84$ kN (–19 kips)
$\Delta M_D = 2$ kN-m (1.5 kip-ft), $\Delta M_G = 111$ kN-m (82 kip-ft)

The change in strain at the level of the post-tensioning tendons is:

$$\varepsilon_{p1} = -838 \times 10^{-6} + 110 \times 10^{-6}/\text{m} \times (1160 - 414) \times 10^{-3}\text{ m} = -756 \times 10^{-6}$$

which is the same value as assumed initially. Similarly, the change in strain at the level of the pretensioning strands is:

$$\varepsilon_{p2} = -838 \times 10^{-6} + 110 \times 10^{-6}/\text{m} \times (1160 - 50) \times 10^{-3}\text{ m} = -716 \times 10^{-6}$$

which is identical to the value initially assumed. Therefore, no further iteration is necessary.

The resulting stresses are shown in Fig. 9 and listed in Table 5 under Case 1a. It is interesting to note that for the girder, the time-dependent stress changes due to differential creep and shrinkage are quite small (rows labeled "CS change" in Table 5). The greater part of the change is due to prestress losses (rows labeled "PT change"). However, it is cautioned that this is not a general conclusion. Creep and shrinkage differentials between deck and girder were greatly reduced for the example

discussed here due to the use of precast deck panels.

The method described above leads to significantly lower predicted prestress losses than would be obtained from the equations given in the AASHTO Standard Specifications.[17] The AASHTO method does not account for a number of factors, including the time of loading and the concrete strength, in the determination of creep and shrinkage losses. Therefore, it will overestimate these losses for girders stressed at a greater age and for higher strength concrete. As noted earlier, the precast girders were required to have a minimum age of 50 days prior to post-tensioning. With this approach, predicted prestress losses could be reduced by 30 percent (181 versus 257 MPa) from the AASHTO predictions.

Sensitivity Analysis

Creep and shrinkage properties observed in actual structures have large scatter caused by the randomness of the material properties and the environment. The 1990 CEB-FIP Model Code[14] gives confidence limits for the equations used for the computation of creep and shrinkage. According to this reference, the creep coefficient at the 90 percent confidence limit may be taken as 1.26 times the expected mean value. Likewise, the 90 percent confidence limit for the shrinkage strain may be taken as 1.45 times the calculated shrinkage strain. Table 5 shows a comparison of the extreme fiber stresses for five different cases:

Case 1a – Mean values for creep and shrinkage, aging coefficient $\mu = 0.7$

Case 1b – Mean values for creep and shrinkage, $\mu = 0.5$

Case 1c – Mean values for creep and shrinkage, $\mu = 0.9$

Case 2 – 90 percent fractile values for both girder and deck, $\mu = 0.7$

Case 3 – 90 percent fractile values for deck, mean values for girder, $\mu = 0.7$

As expected, the combination with the greatest difference in creep and shrinkage properties between girder and deck (Case 3) shows the greatest increase in bottom fiber stress due to creep and shrinkage (Row "CS change" for girder in Table 5). Case 2, which has the highest creep and shrinkage values for the girder, shows the largest stress increase in bottom fiber stresses due to the attendant higher prestress losses (Row "PT change" for girder in Table 5). Comparing the variability of results for Cases 1a, 1b, and 1c to Cases 2 and 3, it is apparent that the randomness of creep and shrinkage properties has a significantly greater influence on the results than the choice of the aging coefficient. Based on the work by Dilger,[5] an aging coefficient of 0.8 is recommended for spliced concrete girder bridges.

Long-Term Deflections

Long-term deflections can be determined by calculating the long-term curvature, κ, for a number of sections along the girder and by subsequent application of the principle of virtual work. Long-term curvatures were found to be approximately linear, with a break at the splice point location. Since post-tensioning forces were nearly symmetrical – due to the influence of wedge seating on one hand, and friction and wobble on the other hand – curvatures had to be determined only for one-half of the girder length. The small contribution of the locally increased curvature over the short length of the closure joints was ignored.

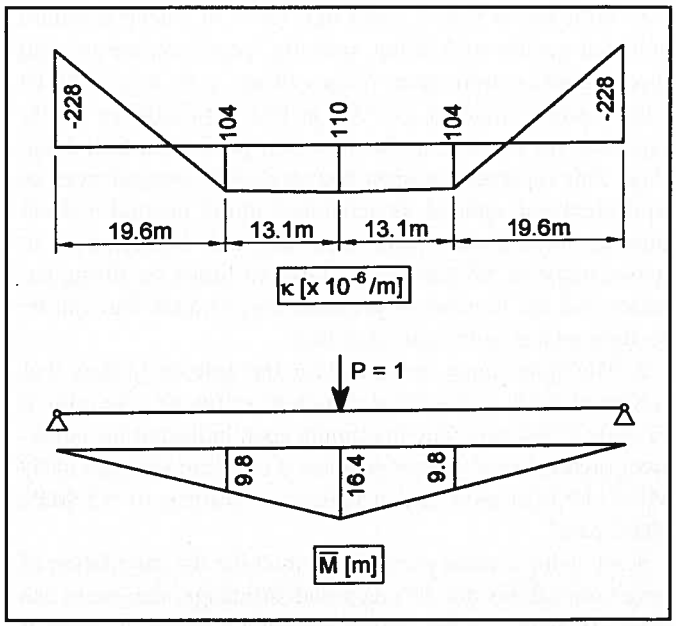

Fig. 10. Long-term curvatures for the composite girder and moment diagram due to a virtual unit force applied at midspan.

Fig. 10 shows a plot of long-term curvatures for the composite girder as well as the moment diagram due to a virtual unit force applied at midspan. Using the principle of virtual work, the long-term change of deflection at midspan is given by Eq. (12):

$$\Delta = \int_{\ell} \kappa(x) \cdot \overline{M}(x)\, dx \qquad (12)$$

where

Δ = midspan deflection

$\kappa(x)$ = curvatures due to long-term effects

$\overline{M}(x)$ = moments due to virtual force applied at midspan

Evaluating the integral in Eq. (12) yields the following midspan deflection:

$$\Delta = 2\left(-228 \cdot 9.8 \cdot \frac{19.6}{6} + 104 \cdot 9.8 \cdot \frac{19.6}{3} + 104 \cdot 9.8 \cdot \frac{13.1}{3} + 104 \cdot 16.4 \cdot \frac{13.1}{6} + 110 \cdot 9.8 \cdot \frac{13.1}{6} + 110 \cdot 16.4 \cdot \frac{13.1}{3}\right) \cdot 10^{-6}$$

$$= 0.036\,\text{m} = 36\,\text{mm}\ (1.4\ \text{in.}) \downarrow$$

Note that, contrary to the typical behavior of precast, pretensioned girders,[3] this long-term deflection is directed downwards. Also note how small the deflection is, given the long span of the structure. The initial deck profile and the support elevations at the temporary towers were adjusted to compensate for these long-term effects.

CONCLUSIONS AND RECOMMENDATIONS

Based on the investigation presented in this paper, the following conclusions and recommendations are offered:

1. With the WSDOT 2400 mm (94.5 in.) deep standard bulb-tee girder, and using splicing, post-tensioning, and shored construction, span ranges of up to 67.4 m (221 ft) with a girder spacing of 2.90 m (9.5 ft) could be easily achieved on the I-15 reconstruction project in Salt Lake City. This represents a span increase of 30 percent over an equivalent non-spliced, pretensioned girder erected without shoring. Such girders have been shown to be restricted to span lengths of 52.4 m (172 ft) due to limits on lifting capacity and the number of pretensioning strands that can be accommodated in the stressing bed.[2]

2. The span range indicated for the spliced girders was achieved with a specified concrete cylinder strength of 52 MPa (7500 psi). The maximum span indicated for equivalent pretensioned girders requires a concrete strength of 69 MPa (10,000 psi) and a release strength of 55 MPa (8000 psi).[2]

3. By using a more accurate method for the calculation of long-term effects due to creep and shrinkage, designers can take advantage of the higher concrete strength at time of post-tensioning and the reduced creep and shrinkage strains from that point onward. This will significantly reduce predicted prestress losses and should result in improved accuracy for camber calculations.

4. The concept of an age-adjusted concrete modulus leads to a relatively simple set of linear equations describing the long-term strains and stress redistributions in a composite section. An aging coefficient of 0.80 is recommended for typical spliced precast concrete girder bridges.

5. The large variability of creep and shrinkage properties should be recognized and may need to be considered in the design of critical applications.

ACKNOWLEDGMENTS

The authors acknowledge the many members of the I-15 design-build team, including the Utah Department of Transportation, the contractor (Wasatch Constructors, a joint venture of Kiewit Construction, Granite Construction, and Washington Construction), and the designers (a joint venture of prime consultants Sverdrup Civil and De Leuw Cather and subconsultants H. W. Lochner, M. K. Centennial, T. Y. Lin International, and URS Corporation). The authors also wish to express their appreciation to the PCI JOURNAL reviewers for their constructive comments.

REFERENCES

1. Shutt, C., "I-15 Project Paves Way for Hybrid Precast Girder," ASCENT, Spring 1999, pp. 24-27.
2. Seguirant, S. J., "New Deep WSDOT Standard Sections Extend Spans of Prestressed Concrete Girders," PCI JOURNAL, V. 43, No. 4, July-August 1998, pp. 92-119.
3. Van Lund, J. A., Kinderman, P. D., and Seguirant. S. J., "New Deep WSDOT Girders Used for the Twisp River Bridge," PCI JOURNAL, V. 47, No. 2, March-April 2002, pp. 21-31.
4. Bazant, Z. P., "Prediction of Concrete Creep Effects Using Age-Adjusted Effective Modulus Method," *ACI Journal,* V. 69, No. 4, April 1972, pp. 212-217.
5. Dilger, H. W., "Creep Analysis of Prestressed Concrete Structures Using Creep-Transformed Section Properties," PCI JOURNAL, V. 27, No. 1, January-February 1982, pp. 98-117.
6. Sattler, K., *Theorie der Verbundkonstruktionen* (Theory of Composite Structures), W. Ernst & Sohn Verlag, Berlin, Germany, 1959 (in German).
7. Tadros, M. K., Ghali, A., and Dilger, W. H., "Time-Dependent Analysis of Composite Frames," *ASCE Journal of the Structural Division,* V. 103, No. 4, April 1977, pp. 871-884.
8. Tadros, M. K., Ghali, A., and Meyer, A. W., "Prestress Loss and Deflection of Precast Concrete Members," PCI JOURNAL, Vol. 30, No. 1, Jan.-Feb. 1985, pp. 114-141.
9. Menn, C., *Prestressed Concrete Bridges*, Birkhäuser Verlag, Basel, 1990.
10. AASHTO, *AASHTO LRFD Bridge Design Specifications,* Second Edition, American Association of State Highway Transportation Officials, Washington, DC, 1998.
11. Nichols, J. J., and Prussack, C., "Innovative Design and Erection Methods Solve Construction of Rock Cut Bridge," PCI JOURNAL, V. 42, No. 4, July-August 1997, pp. 42-55.
12. Ahmad, M. A.-K., and Tadros, M. K., "State-of-the-Art of Precast/Prestressed Concrete Spliced I-Girder Bridges," PCI Committee on Bridges, October 1992, 133 pp.
13. ACI Committee 209, "Prediction of Creep, Shrinkage, and Temperature Effects in Concrete Structures," ACI-209R-82, American Concrete Institute, Farmington Hills, MI, 1982.
14. CEB-FIP Model Code for Concrete Structures, Comité Euro-International du Béton-Fédération International de la Précontrainte, Lausanne, Switzerland, 1990.
15. CEB-FIP Model Code for Concrete Structures, Comité Euro-International du Béton-Fédération International de la Précontrainte, Lausanne, Switzerland, 1978.
16. Collins, M., and Mitchell, D., *Prestressed Concrete Structures*, Prentice Hall, Upper Saddle River, NJ, 1991.
17. AASHTO, *Standard Specifications for Highway Bridges*, Sixteenth Edition, American Association of State Highway Transportation Officials, Washington, DC, 1996.

APPENDIX — NOTATION

A_C = area of transformed composite section
A_D, A_G = area of deck and girder, respectively
A_{ps} = cross sectional area of prestressing steel
a = distance between centroid of deck and centroid of girder
a_D = distance between centroid of deck and centroid of composite section
a_G = distance between centroid of girder and centroid of composite section
E_0, $E(\tau)$ = modulus of elasticity at times t_0 and τ, respectively
E_D, E_G = modulus of elasticity of deck and girder, respectively
E_{ps} = modulus of elasticity of prestressing steel
e = eccentricity of prestressing steel relative to centroid of composite section
f_{pi} = initial stress in prestressing steel
f_{pu} = nominal breaking stress of prestressing steel
I_C = moment of inertia of transformed composite section
I_D, I_G = moment of inertia of deck and girder, respectively, about their own centroids
M_D, M_G = moments in deck and girder
M_D^0, M_G^0 = moments in deck and girder at beginning of composite action
$\overline{M}(x)$ = moment diagram due to virtual force
N_D, N_G = axial loads in deck and girder (tension positive)
N_D^0, N_G^0 = axial loads in deck and girder at begin of composite action
n = modular ratio of deck concrete to girder concrete
S_C = first area moment of transformed deck section about centroid of composite section
t = time interval in hours (for relaxation loss calculations)
t = time at end of creep and shrinkage interval considered in days (for creep and shrinkage strain calculations)
t_0 = time at beginning of creep and shrinkage
Δ = midspan deflection
Δf_R = prestress loss due to strand relaxation
Δf_p = prestress loss due to creep and shrinkage
ΔM_D, ΔM_G = time-dependent change of moments in deck and girder
ΔM_1^p = change of moment due to prestress losses in post-tensioning tendons
ΔM_2^p = change of moment due to prestress losses in pretensioning strands
ΔM_D^p, ΔM_G^p = change of moments in deck and girder due to prestress losses
ΔN_D, ΔN_G = time-dependent change of axial loads in deck and girder (tension positive)
ΔN^p = change of axial load due to prestress losses
ΔN_1^p = change of axial load due to prestress losses in post-tensioning tendons
ΔN_2^p = change of axial load due to prestress losses in pretensioning strands
ΔN_D^p, ΔN_G^p = change of axial load in deck and girder due to prestress losses
ε_D, ε_G = time-dependent strains in deck and girder
ε_{p1} = time-dependent strain at location of centroid of post-tensioning tendons
ε_{p2} = time-dependent strain at location of pretensioning strands
ε_{sD}, ε_{sG} = shrinkage strain for deck and girder
$\varepsilon_{s,t}$ = shrinkage strain at time t
ε_t = total strain at time t
φ_D, φ_G = creep coefficient for deck and girder
φ_{t,t_0} = creep coefficient at time t due to load applied at time t_0
$\varphi(t, \tau)$ = creep coefficient at time t due to load applied at time τ
κ = curvature due to long-term effects
κ_D, κ_G = curvature of deck and girder due to long-term effects
μ = aging coefficient
σ_0 = stress at time t_0
σ_t = stress at time t
$\sigma(\tau)$ = stress at time τ
τ = time variable